Technology in Cancer Research & Treatment
ISSN 1533-0346
Volume 4, Number 5, October (2005)

Thermoacoustic and Photoacoustic Tomography of Thick Biological Tissues Toward Breast Imaging

www.tcrt.org

Geng Ku, Ph.D.[1]
Bruno D. Fornage, M.D.[2]
Xing Jin, M.S.[1]
Minghua Xu, Ph.D.[1]
Kelly K. Hunt, M.D.[3]
Lihong V. Wang, Ph.D.[1,*]

[1]Optical Imaging Laboratory
Department of Biomedical Engineering
Texas A&M University
3120 TAMU
College Station, TX 77843-3120, USA
[2]Departments of Diagnostic Radiology and Surgical Oncology
The University of Texas
M. D. Anderson Cancer Center
Houston, TX 77030, USA
[3]Department of Surgical Oncology
The University of Texas
M. D. Anderson Cancer Center
Houston, TX 77030, USA

* Corresponding Author:
Lihong V. Wang, Ph.D.
Email:LWang@tamu.edu

Microwave-based thermoacoustic tomography (TAT) and laser-based photoacoustic tomography (PAT) in a circular scanning configuration were both developed to image deeply seated lesions and objects in biological tissues. Because malignant breast tissue absorbs microwaves more strongly than benign breast tissue, cancers were imaged with good spatial resolution and contrast by TAT in human breast mastectomy specimens. Based on the intrinsic optical contrast between blood and chicken breast muscle, an embedded blood object that was 5 cm deep in the tissue was also detected using PAT at a wavelength of 1064 nm.

Introduction

Thermoacoustic tomography (TAT) and photoacoustic tomography (PAT), based on the measurement of ultrasonic waves induced by electromagnetic pulses, can reveal dielectric or optical properties of tissues that are closely related to the physiological and pathological status of the tissues (1-4). TAT uses electromagnetic radiation in the radiofrequency (RF) or microwave bands, while PAT employs visible or near infrared (NIR) light. These novel non-invasive and non-ionizing imaging modalities can potentially provide high imaging contrast based on a tissue's rate of absorption of electromagnetic radiation. Cancer diagnosis based on information from tissue properties over an electromagnetic spectrum from RF to optical bands can potentially be more accurate than has previously been available. In this paper, we report on our preliminary study of deep imaging using microwave and NIR radiation.

Electromagnetic energy is absorbed by biological tissues when an electromagnetic pulse, such as a microwave or laser pulse, is used to irradiate the tissues. Absorption of the electromagnetic energy generates heat and the subsequent expansion that causes the emission of acoustic waves, which is called the thermoacoustic effect. This phenomenon of microwaves was known as the microwave-auditory or the microwave-hearing effect in the electromagnetically lossy media previously (5). Figure 1 shows the absorption coefficient of water to electromagnetic waves of frequencies ranging from 3×10^7 to 3×10^{16} Hz (6), that of whole blood to visible and near infrared light (7, 8), and those of some human tissues to microwaves (1, 2). Water has little absorption to visible light while hemoglobin in blood dominates the optical absorption in most soft tissues. In the microwave range, water content in tissue dominates its absorption to electromagnetic energy. Cancerous breast tissues are 2-5 times more absorbing than surrounding normal breast tissues, which has been attributed to an increase in bound water and sodium within malignant cells (1, 9, 10).

Several investigators employed microwave-induced thermoacoustics in the 1980s to image biological tissues (11-16). These early works did not produce

tomographic images but proved that microwave induced thermoacoustic signals could be used for imaging purposes. Later, depth-resolved images in biomedical tissues were computationally reconstructed (17-19), or directly formed by the linear scanning of a focused ultrasound transducer; the latter is similar to an ultrasonic B-scan, except that the ultrasound is produced inside the tissue by microwave pulses (20-22). Kruger *et al*. reported on thermoacoustic breast cancer imaging *in vivo* and referred to it as thermoacoustic CT (23, 24). Reconstruction algorithms based on various scanning configurations were extensively studied and images were improved over time (25-28).

Laser technology has provided a useful short-pulsed and wavelength-tunable light source for PAT. At some wavelengths of light, the absorption coefficient of blood can be ten times higher than that of its surrounding tissues, which results in excellent intrinsic contrast for blood-vessel imaging. PAT has been successfully applied to imaging vascular structures and tumor angiogenesis a few mm under the skin (29-32). Due to the strong optical scattering effect in biological tissues that enhances the effective optical absorption, light intensity, and hence photoacoustic strength, decreases with depth approximately exponentially, with a decay constant of a few mm. To reach deeper tissue structures, NIR is a better excitation source since it has a low absorption coefficient and a relatively low scattering coefficient in biological tissues and can, consequently, provide deeper penetration. Esenaliev *et al*. studied the imaging sensitivity of PAT on deeply embedded objects using tissue phantoms (33), and Oraevsky *et al*. reported a PAT image of a ductal carcinoma at a depth of about 1.1 cm from the breast surface using the 1064-nm wavelength (34, 35).

Thermoacoustic and photoacoustic imaging techniques are based on ultrasonic propagation and detection, which means that they have the same good spatial resolution as pure ultrasound imaging. The geometry of the region over which the ultrasonic transducer is scanned determines the imaging mode and the reconstruction algorithms. For the detection of layered structures of tissues or tumors near human epidermis, the ultrasonic transducer can be placed on the skin along the laser beam to accomplish detection *in vivo*. Karabutov *et al*. (36, 37) presented photoacoustic imaging in backward mode detection. Maslov *et al*., using a 2D linear scan configuration, clearly imaged the vascular structures under rat skin *in vivo* (38). The imaging of small deeply embedded tumors, such as breast tumors, was also studied by Esenaliev and Oraevsky *et al*. (33, 39). Hoelen *et al*. employed a transducer array on a plane to detect induced signals from vascular systems (40). The image was reconstructed using a delay-and-sum algorithm, where the depth resolution was better than 20 μm, and the lateral resolution was better than 200 μm. A detector can also be scanned over a circular track

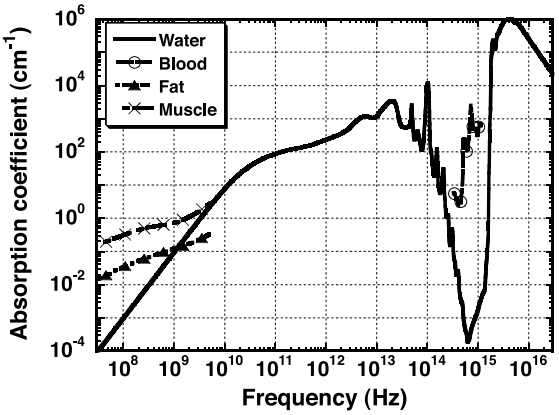

Figure 1: Absorption spectra of water and various biological tissues versus the electromagnetic frequency.

around a test sample to collect transversally propagating acoustic waves. A photoacoustic image is then reconstructed using the detected signals. This configuration allows us to image deep tissue structures (41). When the optical penetration is optimized with near-infrared laser pulses of 800 nm in wavelength, the optical contrast is enhanced by indocyanine green (ICG) whose absorption peak matches the laser wavelength. This optimized PAT is able to image fine vascular-like objects embedded at a depth of up to 5 cm, at a resolution of less than about 780 microns with a sensitivity of <7 pmol of ICG in blood (42).

Materials and Methods

Both of the deeply penetrating TAT and PAT imaging systems are shown in Figure 2. TAT, based on the detection of microwave pulse-induced acoustic signals, was applied to imaging mastectomy specimens – excised whole breasts. PAT, using a short laser pulse for excitation, was used to image deeply embedded objects in tissue samples as an initial step toward breast imaging.

The microwave pulses transmitted from a 3-GHz microwave generator were delivered to the sample through a rectangu-

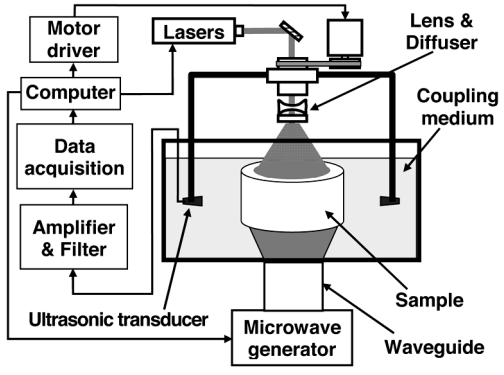

Figure 2: Schematic of deeply penetrating thermoacoustic and photoacoustic tomography.

lar waveguide and then an air-filled pyramidal horn antenna with an opening of 120 mm × 88 mm. The pulse repetition rate was set to around 50 Hz for the imaging. The pulse width was measured to be 0.5 μs, and the pulse energy was estimated to be 15 mJ. The TAT and PAT systems both had four independent detection channels that could simultaneously receive thermoacoustic signals through four ultrasonic transducers. It is difficult to achieve both high imaging resolution (bandwidth) and high sensitivity using a single ultrasonic transducer. Hence, ultrasonic transducers with different central frequencies are employed to expand the detection bandwidth. Our TAT and PAT systems are capable of simultaneously imaging with multiple detection channels, which allows us to employ various ultrasonic transducers and optimize the detection parameters more efficiently. In the thermoacoustic imaging, the heights of the four ultrasonic transducers were adjusted to approximately match the height of the tumor in the breast. Two channels used two cylindrically focused (in the elevation dimension) ultrasonic transducers with central frequencies of 1 MHz (V3014/1-MHz, Panametrics) and 3.5 MHz (V383/3.5-MHz, Panametrics), respectively. The other two channels used two unfocused ultrasonic transducers with central frequencies of 1 MHz (V3015/1-MHz, Panametrics) and 2.25 MHz (V323/2.25-MHz, Panametrics), respectively. The diameters of their active elements were 2.5 cm, 0.6 cm, 0.6 cm, and 1 cm for the 1-MHz cylindrical, 1-MHz flat, 2.25-MHz flat, and 3.5-MHz cylindrical transducers, respectively. The transducers were fastened to a rotational apparatus and immersed in mineral oil in a plastic container. A step motor drove the rotational apparatus and then scanned the transducers around the sample along a horizontal circle with a step size of 1.5° with the transducers always pointing horizontally to the rotation center during the scanning. The ultrasonic transducers converted the thermoacoustic energy into electronic signals, which were then amplified and filtered electronically. The electronic signals were recorded by an oscilloscope (TDS640A, Tektronix), averaged 100 times at each scanning stop, and finally transferred to a computer for imaging based on our back-projection algorithms. The sampling frequency of the oscilloscope was set to 20 or 50 MHz. Each scanning took approximately 15 minutes.

In the experiment of imaging mastectomy specimens, we followed the procedures outlined below. First, mammograms were taken at M. D. Anderson Cancer Center as a standard component of the patient's diagnostic workup. A mammogram reflects the different attenuations of an x-ray beam within a patient's breast. Therefore, the image contrast produced by an object depends on the attenuation of the x-ray beam relative to the attenuation of the background tissue. To improve the contrast, the breast is often x-rayed under compression. After surgery, the mastectomy specimen was placed in an approximately cylindrical plastic container with the nipple facing down. The 12 o'clock and 3 o'clock positions were marked on the rim of the container. A layer of mineral oil was applied to the inner wall of the container to facilitate the coupling of thermoacoustic signals through it. A vacuum pump was also used to remove air bubbles in the mineral oil between the tissue sample and the container's wall so that good acoustic coupling could be achieved. The diameter of the container in the horizontal thermoacoustic imaging plane were 11 and 17 cm, respectively, in our two reported cases. The thicknesses of the specimens in the container are 9 and 4 cm, respectively, depending on the specimen size. Next, a conventional B-mode gray-scale sonogram of the specimen was taken using a real-time scanner (HDI 5000, Philips-ATL, Bothell, WA) equipped with a 5-12 MHz broadband linear array electronic transducer. Then, the specimen was imaged using our thermoacoustic imaging system. Finally, another radiograph of the specimen was taken from the top of the cylindrical container to compare the result in the thermoacoustic image with that in the mammograms, the latter being considered the golden standard of breast imaging. After these imaging experiments, the specimen was restituted to the Department of Pathology for histopathological diagnosis.

In the PAT mode, a pulsed Ti: Sapphire laser (LOTIS TII, Symphotic), which is pumped by a Q-switched Nd: YAG laser at a repetition rate of 10 Hz, provided about 10-ns tunable NIR laser pulses. The laser system can provide 120 mJ and 1000 mJ maximal output energy at wavelengths of 800 nm and 1064 nm, respectively. The laser beam was expanded by a concave lens, homogenized by a ground glass and then directed onto a sample. The incident laser energy densities on the tissue surface were about 7 mJ/cm^2 and about 60 mJ/cm^2 for the above two near-infrared wavelengths, respectively. Four ultrasonic transducers (V323/2.25-MHz, V383/3.5-MHz, V157/5-MHz, and V312/10-MHz, Panametrics), with nominal bandwidths ranging from 50% to 80% of their specified central frequencies, were used for detection in four different frequency ranges. The diameters of their active elements were 0.6 cm, 1 cm, 0.3 cm, and 0.6 cm for the 2.25-MHz, 3.5-MHz, 5-MHz, and 10-MHz transducers, respectively. The 3.5-MHz transducer was cylindrically focused in the elevation dimension while the others had flat active surfaces. In the photoacoustic imaging test, the sample and the transducers were immersed in a tank of water for coupling the photoacoustic waves to the transducers. Chicken breast muscle was used as the test sample, and an object was made by pouring raw rat blood into a transparent plastic tube that had an inner diameter of 1.5 mm.

Results and Discussion

A tissue sample made of porcine fat with porcine tendon and muscle columns embedded was imaged with both TAT and PAT. The white tendon taken from a porcine foot did not look

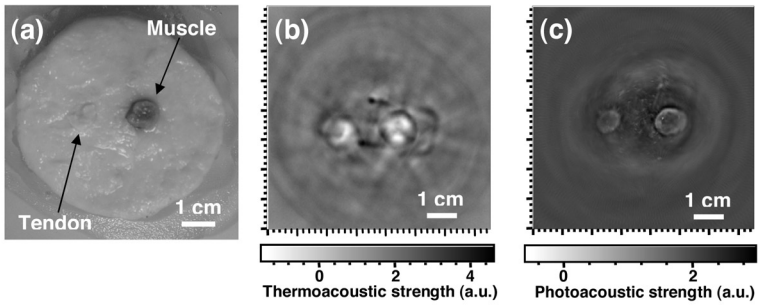

Figure 3: Thermoacoustic and photoacoustic images of porcine muscle and tendon in fat tissue. (**a**) Photograph of the tissue sample. (**b**) Thermoacoustic image. A U-shaped metal wire placed on the tissue sample was imaged along with the muscle and tendon. (**c**) Photoacoustic image.

significantly different from the fat tissue on a conventional photograph [Fig. 3(a)]. Both tendon and muscle tissues have stronger absorption to microwave than fat because of their higher water concentration, hence present high contrast in the thermoacoustic tomograph [Fig. 3(b)]. A U-shaped copper wire was put inside the test sample to label the orientation of the object and was imaged along with the two embedded objects. Although the tendon had obviously weaker optical absorption than the muscle; it was nevertheless clearly shown in the photoacoustic image [Fig. 3(c)]. Comparing the images obtained from microwave and laser excitations, we demonstrated that thermoacoustic and photoacoustic tomographies reveal tissue's absorption to microwave and optical radiations, respectively, along with their thermoelastic properties. The boundary of the object in the thermoacoustic image is not as sharp as that in the photoacoustic image. This

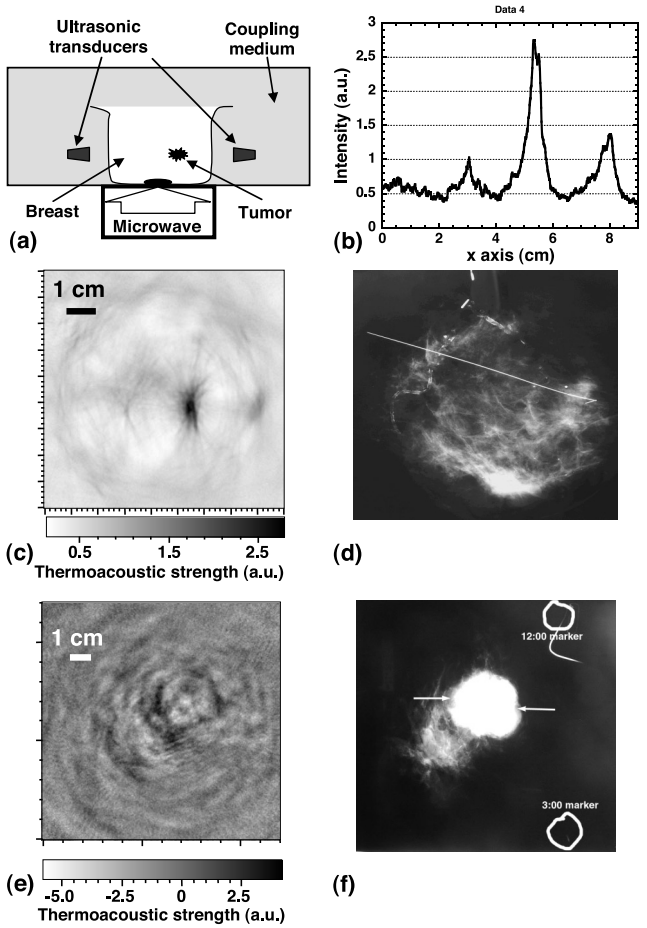

Figure 4: Thermoacoustic images of two excised whole breasts (mastectomy specimens). (**a**) Schematic of thermoacoustic tomography of a mastectomy specimen. (**b**) One-dimensional thermoacoustic imaging across a tumor region. (**c**) Thermoacoustic image of one mastectomy specimen. Darker area indicates higher microwave absorption in cancerous region. (**d**) Digital radiograph of the mastectomy specimen with the same view orientation as in (**c**). The white line is a localizing wire placed into the lesion for sample orientation. (**e**) Thermoacoustic image of another mastectomy specimen. (**f**) Digital radiograph of the mastectomy specimen with the same view orientation as in (**e**).

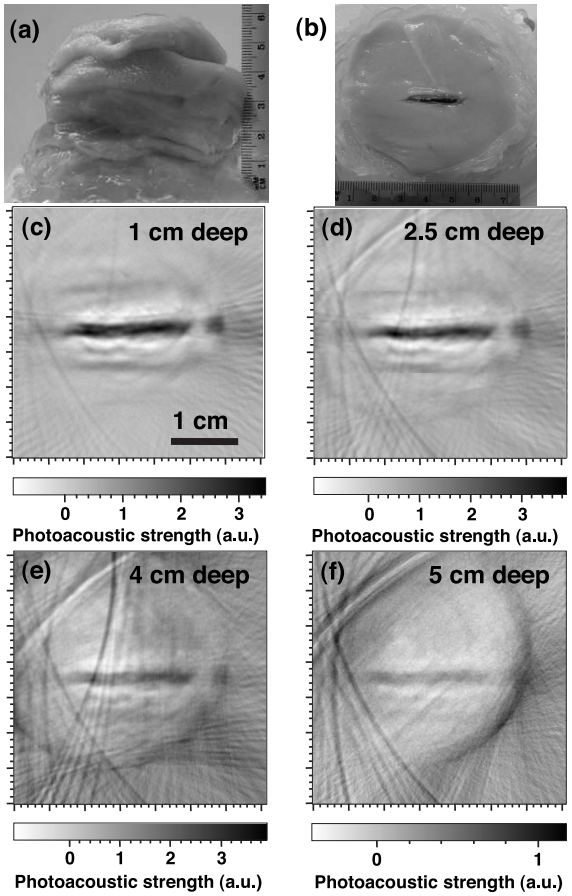

Figure 5: Two-dimensional photoacoustic images of a blood object in chicken breast muscle. Photograph of (**a**) the entire test sample and (**b**) the blood object embedded in a cross section of chicken breast muscle. Two-dimensional photoacoustic images acquired with a 3.5-MHz ultrasonic transducer at depths of (**c**) 1 cm, (**d**) 2.5 cm, (**e**) 4 cm, and (**f**) 5 cm, respectively, in chicken breast muscle.

appearance reveals the difference in imaging resolution because of the longer microwave pulse width compared with the laser pulse width. The signals measured by an ultrasonic transducer mainly exist in a bandwidth near the ultrasonic transducer center frequency. The DC and very low frequency components of the induced acoustic signal are filtered out. Therefore, only those features of an object corresponding to the recorded signal are reconstructed, leading to an enhanced boundary of an object in general.

The thermoacoustic images of two mastectomy specimens are compared with the corresponding radiographs in Figure 4. Using the thermoacoustic signals detected by the transducers which were scanned around the breast [Fig. 4(a)], the thermoacoustic images from the four detection channels were reconstructed and compared. In the breast with a lesion that was later pathologically diagnosed as infiltrating lobular carcinoma, a strong contrast was observed in the images from all four channels with consistency in tumor position and shape. Figure 4(b) illustrates a typical one-dimensional image across the tumor region. The tumor-to-background contrast was estimated to be about 5:1, which demonstrates the method's imaging contrast advantage over the few-percent contrast obtained with x-ray mammograms. Among the four simultaneously acquired images, the two focused transducers provided higher signal-to-noise ratios. The thermoacoustic image of the breast captured by the 1-MHz focused transducer is shown in Figure 4(c). The dark area represents stronger microwave absorption, which indicates a cancerous area as the digital radiograph of the same specimen [Fig. 4(d)] identified the similar tumor location and size as in our thermoacoustic image. The object was measured to be approximately 12 mm × 20 mm in the horizontal imaging plane and located about 2 cm above the container bottom. The thickness of this specimen was about 9 cm in an 11 cm diameter container. The size of the tumor on the radiograph was about 26 mm × 15 mm.

Figures 4(e) and 4(f) show the thermoacoustic image and the digital radiograph, respectively, of another mastectomy specimen. This specimen was imaged similarly as the previous specimen. The diameter of the container in the horizontal thermoacoustic imaging plane was 17 cm in this case. The thickness of this specimen was about 4 cm. The distance of the tumor from the bottom was measured by conventional ultrasound imaging to be about 1.8 cm. The thermoacoustic image [Fig. 4(e)] was reconstructed from data detected by a 2.25-MHz cylindrically focused ultrasonic transducer. A stronger microwave absorption object located at the center was identified. The object was assumed to correlate with the known tumor and measured at about 35 mm in diameter. The average tumor-to-background contrast in this thermoacoustic image was estimated to be about 3.5:1, which is again much greater than the contrast in x-ray mammograms. The size of the tumor on the radiograph was about 36 mm in diameter. This lesion was pathologically diagnosed as an invasive metaplastic carcinoma with chondroid and squamous metaplasia. Again, the digital radiograph [Fig. 4(f)] of the same specimen verified the tumor location and size in our thermoacoustic image [Fig. 4(e)].

Photoacoustic tomography can be used to detect tumors by imaging tumor-related vasculatures, such as angiogenesis, and hemorrhagic infiltration. To demonstrate the potential of PAT for imaging deep vessels, PAT images of raw blood in a 1.5 mm diameter tube at different tissue depths up to 5 cm are compared in Figure 5. The photographs of the entire sample and the cross section containing the embedded object are shown in Figures 5(a) and (b), respectively. The tissue's cross section containing the embedded blood object was imaged with four pieces of chicken breast tissue sequentially stacked up, which placed the embedded objects 1 cm, 2.5 cm, 4 cm, and 5 cm, respectively, away from the laser illuminated tissue surface. Figures 5(c) to (f) show the PAT images acquired by the 3.5-MHz transducer at each depth. The blood object was clearly imaged when it was 1 cm and 2.5 cm below the laser illuminated surface. At a depth of 4 cm, the blood was still clearly visible although there was some interference spoiling the image. When the fourth chicken tissue sample of 1 cm in thickness was stacked on, making the blood object 5 cm deep, the blood object became obscured. The photoacoustic images of the blood at each depth show that the image width was maintained at around 2 mm at a depth of less than 4 cm and increased slightly at a depth of 5 cm. In the longitudinal direction, there was a dark spot lying away from the right end of the blood column in the image. We discovered later that there was a bubble at the corresponding position inside the tube, which separated the blood column into two parts. This sample fault is clearly revealed by the photoacoustic imaging.

Since the photoacoustic signal was proportional to the laser light intensity; the photoacoustic signal amplitude as a function of depth can be used to measure the light attenuation. The light intensities that transmitted through the four tissue thicknesses were also detected using a photodiode detector (DET110, Thorlabs). The effective attenuation coefficient of the chicken breast tissue was fitted to be 1.2 cm^{-1} based on Beer's law. Therefore, the 5 cm maximum imaging depth amounted to approximately 6 times the 1/e optical penetration depth, corresponding to a 26-dB attenuation from the incident to the transmitted optical energy density. This light attenuation in chicken breast muscle is similar to that in some human breast tissue, which shows a wide range in optical properties depending on different human groups (4, 43). Real breast tumors and angiogenesis are most likely less absorptive than the blood object used in the PAT experiment here and will produce weaker photoacoustic signals. To obtain a photoacoustic image from a comparable

depth, optical contrast agent should be used to enhance the optical absorption of the target.

Conclusion

Using microwave and NIR laser light as excitation sources improved imaging depth because of their deep penetration into biological tissues. Carcinomas located about 2 cm deep in mastectomy specimens were clearly imaged by TAT. A blood object embedded in 5 cm deep tissue was disclosed based on the tissue's intrinsic contrast by PAT. While this looks very promising for breast tumor imaging, our preliminary results also suggest that this imaging modality can be further developed to detect tissue absorption properties over an electromagnetic spectrum in both the RF and the optical regions, and thereby, become a spectral and functional imaging modality that can be potentially used for early breast tumor diagnosis. Multiple ultrasonic transducers were simultaneously used to cover both the detection sensitivity and image resolution, which allowed us to optimize the detection parameters more efficiently.

Acknowledgements

We thank G. Stoica for assistance with blood samples and X. Xie, X. Wang, M. Sivaramakrishnan, and K. Song for lab assistance. This study is sponsored in part by the National Institute of Health grants R01 EB000712 and R01 NS46214 and the Texas ARP grant 000512-0063-2001.

References

1. S. Chaudhary, R. Mishra, A. Swarup, and J. Thomas. Dielectric Properties of Normal & Malignant Human Breast Tissues at Radiowave and Microwave Frequencies. *Indian J. Biochem. Biophys. 21*, 76-79 (1984).
2. W. Joines, R. Jirtle, M. Rafal, and D. Schaeffer. Microwave Power Absorption Differences Between Normal and Malignant Tissue. *Radiation Oncology-Biology-Physics. 6*, 681-687 (1980).
3. W. Joines, Y. Zhang, C. Li, and R. Jirtle. The Measured Electrical Properties of Normal and Malignant Human Tissues from 50-900 MHz. *Medical Physics. 21*, 547-550 (1994).
4. W. F. Cheong, S. A. Prahl, and A. J. Welch. A Review of the Optical Properties of Biological Tissues. *IEEE J. Quantum Elect. 26*, 2166-2185 (1990).
5. J. C. Lin. On Microwave-Induced Hearing Sensation. *IEEE Trans. Microwave Theory Tech. 25*, 605-613 (1977).
6. D. J Segelstein. *The Complex Refractive Index of Water*. M.S. Thesis. Department of Physics, University of Missouri-Kansas City, Kansas City, Mo. (1981).
7. Scott Prahl. Tabulated Molar Extinction Coefficient for Hemoglobin in Water. http://omlc.ogi.edu/spectra/hemoglobin/summary.html (2005)
8. W. G. Zijlstra, A. Buursma, and O. W. van Assendelft. *Visible and Near Infrared Absorption Spectra of Human and Animal Haemoglobin*. VSP, Netherlands (2000)
9. W. Joines, R. Jirtle, M. Rafal, and D. Schaeffer. Microwave Power Absorption Differences Between Normal and Malignant Tissue. *Radiation Oncology-Biology-Physics 6*, 681-687 (1980).
10. W. Joines, Y. Zhang, C. Li, and R. Jirtle. The Measured Electrical Properties of Normal and Malignant Human Tissues from 50-900 MHz. *Medical Physics 21*, 547-550 (1994).
11. T. Bowen, L. Nasoni, A. E. Pifer, and G. H. Sembrosk. In *Proc. IEEE Ultrasonics Symposium 2*, 823-827 (1981).
12. J. P. Powers, Ed. *Acoustic Imaging*. Plenum Publishing, New York (1982).
13. R. G. Olsen and J. C. Lin. Acoustic Imaging of a Model of a Human Hand Using Pulsed Microwave Irradiation. *Bioelectromagnetics. 4*, 397-400 (1983).
14. J. C. Lin and K. H. Chan. Microwave Thermoelastic Tissue Imaging System Design. *IEEE Trans. Microwave Theory Tech. 32*, 854-860 (1984).
15. R. L. Nasoni, G. A. Evanoff, Jr., P. G. Halverson, and T. Bowen. Thermoacoustic Emission by Deeply Penetrating Microwave Radiation. In *Proc. IEEE Ultrasonics Symposium 5*, 633-637 (1984).
16. K. H. Chan and J. C. Lin. Microwave-Induced Thermoacoustic Tissue Imaging. In *Proc. Engineering in Medicine and Biology Society 10th Annual International Conference*. pp. 445-446 (1988).
17. R. A. Kruger, P-Y. Liu, and Y. Fang. Photoacoustic Ultrasound (PAUS) – Reconstruction Tomography. *Med. Phys. 22*, 1605-1609 (1995).
18. R. A. Kruger, K. K. Kopecky, A. M. Aisen, D. R. Reinecke, G. A. Kruger, and W. L. Kiser, Jr. Thermoacoustic CT with Radio Waves: A Medical Imaging Paradigm. *Radiology. 211*, 275-278 (1999).
19. R. A. Kruger, D. R. Reinecke, and G. A. Kruger. Thermoacoustic Computed Tomography-Technical Considerations. *Med. Phys. 26*, 1832-1837 (1999).
20. L.-H. Wang, X. Zhao, H. Sun, and G. Ku. Microwave-Induced Acoustic Imaging of Biological Tissues. *Rev. Sci. Instrum. 70*, 3744-3748 (1999).
21. G. Ku and L.-H. Wang. Scanning Thermoacoustic Tomography in Biological Tissue. *Med. Phys. 27*, 1195-1202 (2000).
22. G. Ku and L.-H. Wang. Scanning Microwave-Induced Thermoacoustic Tomography: Signal, Resolution, and Contrast. *Med. Phys. 28*, 4-10 (2001).
23. R. A. Kruger and W. L. Kiser, Jr. Thermoacoustic CT of the Breast: Pilot Study Observations. *Proc. SPIE 4256*, 1-5 (2001).
24. R. A. Kruger, K. Stantz, and W. L. Kiser, Jr. Thermoacoustic CT of the Breast. *Proc. SPIE 4682*, 521-525. (2002).
25. K. P. Kostli, M. Frenz, H. Bebie, and H. P. Weber. Temporal Backward Projection of Optoacoustic Pressure Transients Using Fourier Transform Methods. *Phys. Med. Biol. 46*, 1863-1872 (2001).
26. M. Xu, and L.-H. Wang. Time-Domain Reconstruction for Thermoacoustic Tomography in a Spherical Geometry. *IEEE Trans. Med. Imag. 21*, 814-822 (2002).
27. Y. Xu, D. Feng, and L.-H. Wang. Exact Frequency-Domain Reconstruction for Thermoacoustic Tomography: I. Planar Geometry. *IEEE Trans. Med. Imag. 21*, 823-828 (2002).
28. Y. Xu, M. Xu, L.-H. Wang. Exact Frequency-Domain Reconstruction for Thermoacoustic Tomography: II. Cylindrical Geometry. *IEEE Trans. Med. Imag. 21*, 829-833 (2002).
29. R. G. M. Kolkman, E. Hondebrink, W. Steenbergen, F. F. M. de Mul. *In Vivo* Photoacoustic Imaging of Blood Vessels Using an Extreme-Narrow Aperture Sensor. *IEEE J. Sel. Top. Quantum Electron. 9*, 343-346, (2003).
30. X. Wang, Y. Pang, G. Ku, X. Xie, G. Stoica, and L.-H. Wang. Non-Invasive Laser-Induced Photoacoustic Tomography for Structural and Functional Imaging of the Brain *In Vivo*. *Nat. Biotechnol. 21*, 803-806 (2003).
31. G. Ku, X. Wang, X. Xie, G. Stoica, L.-H., and V. Wang. Multiple-Bandwidth Photoacoustic Tomography. *Phys. Med. Biol. 49*, 1329-1338 (2004).
32. G. Ku, X. Wang, X. Xie, G. Stoica, and L. -H. Wang. Imaging of Tumor Angiogenesis in Rat Brains *In Vivo* by Photoacoustic Tomography. *Applied Optics 44*, 770-775 (2005).

33. R. O. Esenaliev, A. A. Karabutov, and A. A. Oraevsky. Sensitivity of Laser Opto-Acoustic Imaging in Detection of Small Deeply Embedded Tumors. *IEEE J. Sel. Top. Quant. 5*, 981-988 (1999).
34. A. A. Karabutov, E. V. Savateeva, and A. A. Oraevsky. Optoacoustic Tomography: New Modality of Laser Diagnostic Systems. *Laser Physics 13*, 711-723 (2003).
35. A. A. Oraevsky, E. V. Savateeva, S. V. Solomatin, A. A. Karabutov, V. G. Andreev, Z. Gatalica, T. Khamapirad, and P. M. Henrichs. Optoacoustic Imaging of Blood for Visualization and Diagnostics of Breast Cancer. In *Biomedical Optoacoustics III 4618*, 81-94. Ed., A. A. Oraevsky (2002).
36. A. A. Karabutov, E. V. Savateeva, N. B. Podymova, and A. A. Oraevsky. Backward Mode Detection of Laser-Induced Wide-Band Ultrasonic Transients with Optoacoustic Transducer. *J. Appl. Phys. 87*, 2003-2014 (2000).
37. A. A. Karabutov, E. V. Savateeva, and A. A. Oraevsky. Imaging of Layered Structures in Biological Tissues with Opto-Acoustic Front Surface Transducer. *Proc. SPIE. 3601*, 284-295 (1999).
38. K. Maslov, G. Stoica, and L.-H. Wang. *In Vivo* Dark-Field Reflection-Mode Photoacoustic Microscopy. *Optics Letters. 30*, 625-626 (2005).
39. R. O. Esenaliev, F. K. Tittel, S. L. Thomsen, B. Fornage, C. Stelling, A. A. Karabutov, and A. A. Oraevsky. Laser Optoacoustic Imaging for Breast Cancer Diagnostics: Limit of Detection and Comparison with X-ray and Ultrasound Imaging. *Proc. SPIE. 2979*, 71-82 (1997).
40. C. G. A. Hoelen and F. F. M. de Mul. Image Reconstruction for Photoacoustic Scanning of Tissue Structures. *Appl. Opt. 39*, 5872-5883 (2000).
41. X. Wang, Y. Pang, G. Ku, G. Stoica, and L.-H. Wang. Three-Dimensional Laser-Induced Photoacoustic Tomography of the Mouse Brain with the Skin and Skull Intact. *Optics Letters 28*, 1739-1741 (2003)
42. G. Ku and L.-H. Wang. Deeply Penetrating Photoacoustic Tomography in Biological Tissues Enhanced with an Optical Contrast Agent. *Optics Letters 30*, 507-509 (2005)
43. V. Tuchin. *Tissue Optics,* p. 33. SPIE, Bellingham, Washington (2000).

Date Received: May 1, 2005
Date Accepted: July 19, 2005